RF Characterization of an Inflatable Parabolic Torus Reflector Antenna for Space-Borne Applications

Robert A. Hoferer, *Student Member, IEEE*, and Yahya Rahmat-Samii, *Fellow, IEEE*

***Abstract*— Space-borne satellite applications provide a vast array of services extending from global connectivity to earth observation systems. The soil moisture radiation mission is a proposed space-borne passive microwave system complementary to the existing earth observing system operating at low microwave frequencies and requiring an antenna with multibeam, high-beam efficiency, and dual polarization capabilities. To achieve both the large reflector size and the multibeam pattern at the operational frequencies an innovative multibeam reflector antenna design was needed. Recent advances in inflatable antenna technology has been proposed to overcome the launch vehicle size and weight restrictions. This paper describes a novel offset parabolic torus reflector antenna design that produces the desired multibeam pattern and is compatible with the inflatable antenna technology. Using the system requirements of this mission as an example, the design process for an inflatable parabolic torus reflector antenna is outlined, the development of suitable distortion models is given, and representative RF characteristics are presented. These RF characteristics include far-field patterns, beam contour patterns, beam efficiency, and other key performance parameters. The development of an advanced analytical modeling/numerical tool in support of the design effort is also detailed.**

***Index Terms*— Inflatable reflector antennas, multibeam, parabolic torus, physical optics, radiometers, satellite antennas.**

I. Introduction

SPACE-BORNE satellite applications have shown a tremendous growth in recent years. The provided and proposed services range from satellite communications to radiometer systems. The soil moisture radiation mission (SMRM) is a proposed novel radiometer system that will enhance the capabilities of the earth observation system (EOS). EOS is part of NASA's Mission to Planet Earth program and intended to provide measurement of the earth's environment (air, water, land, and biota). The objective of the SMRM is to collect global data of the earth surface using a multibeam antenna system with a passive microwave system at two frequencies and two polarizations [1]. This measurement is used to determine land–surface soil moisture, ocean salinity, surface temperature, and vegetation water content. With operating frequencies in L-band (1.4 GHz) and S-band (2.56 GHz), global measurement in a two-day cycle with high spatial resolution (30 km) and high-beam efficiency is required. Some of the key design parameters of this mission are listed in Fig. 1. Initial studies indicated that the required antenna system would be too large and too heavy if conventional technologies were employed. An alternate means of achieving the mission requirement was needed.

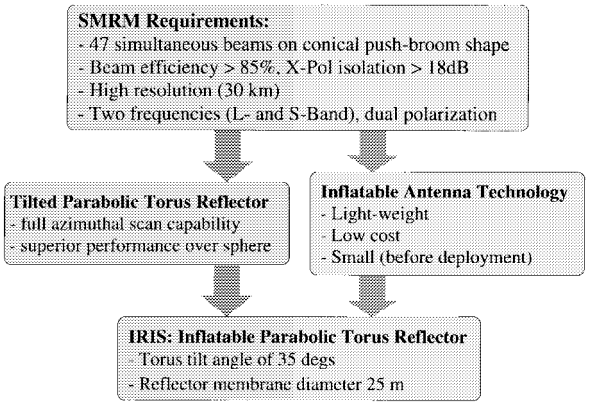

Fig. 1. Diagram detailing the SMRM requirements, the benefits of using IAT, and PTRA in order to meet the design requirements.

A. Inflatable Antenna Technology and Tilted Parabolic Torus

To meet the requirements of both a large antenna size and a reflector shape capable of producing a multibeam pattern, two novel approaches were investigated. These two approaches are referred to as *inflatable antenna technology* and *tilted parabolic torus reflector* and are detailed in the following. Some unique features of these two approaches are listed in Fig. 1.

The deployment of space-borne reflector antennas operating at low frequencies is restricted by the maximum payload weight and dimensions allowed by the launch vehicle. Recent advances in inflatable antenna technology (IAT) provide a unique opportunity to consider the application of large reflector antennas in space [2]. An inflatable antenna is small in size before deployment and extremely light weight, hence, the size and weight limitations of the launch vehicle can be accommodated. Additionally, inflatable antennas are inherently low in cost [2].

For the SMRM, the inflatable reflector antenna shape that best meets the multibeam pattern requirements of this mission was found to be a parabolic torus with an inclined torus tilt axis. The rotational symmetry of this antenna provides natural 360° azimuthal beam scanning capabilities without beam degradation experienced by a paraboloid. Compared to a spherical reflector, the parabolic torus reflector antenna

Manuscript received September 22, 1997; revised April 9, 1998. This work was supported in part by JPL Contract 960591.

The authors are with the Department of Electrical Engineering, University of California, Los Angeles, CA 90095 USA.

Publisher Item Identifier S 0018-926X(98)07492-4.

Fig. 2. An artist's rendition of IRIS in orbit around earth. The reflector is an inflatable parabolic torus with a tilt angle of 35°.

(PTRA) has a superior radiation performance since in one plane the function defining the surface is a parabola.

The combination of IAT and PTRA was named inflatable radiometer imaging system (IRIS). Fig. 2 displays an artist's rendition of IRIS in orbit around earth. Reflector membrane, canopy, feed membrane, the supporting inflatable struts, and the satellite bus are shown. A ray tube emanated from earth, reflected off the reflector membrane, and received by the array feeds is outlined and the conical push-broom shape of the multibeam pattern is sketched by its footprint on the earth surface in Fig. 2.

C. Key Contributions

In order to fully understand the electromagnetic properties of IRIS, it was necessary to develop an advanced computational tool. Since the antenna radiation properties are dependent on the geometrical parameters of IRIS the computational tool had to include the ability to handle systematic and random surface distortions expected in the IRIS configuration.

To analyze the radiation performance of IRIS, a customized version of physical optics (PO) is used. In Section II of this paper, the surface description and surface normal vector necessary for PO application are derived for an offset parabolic torus and a brief derivation of far-field PO is given. In Section III, the most suitable antenna configuration is presented based on system design requirements such as torus tilt angle, desired resolution, and maximum dimensions. Since large structures in space are subject to various distortions [3], [4], a detailed understanding of the effects of these distortions on the radiation performance is necessary. Assuming the deformations of the inflatable structure due to satellite movement or inflation process die out sufficiently fast, static deformations of the inflatable structure are the primary surface distortions that must be accounted for. To be able to investigate the influence of surface distortions on the radiation characteristics, suitable distortion models for IRIS are developed in Section IV in order to accurately simulate the radiation characteristics of a distorted structure.

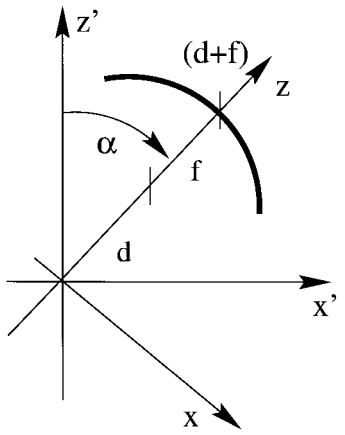

Fig. 3. Parabola with a focal length f and a focus offset d, tilted about the $\hat{\mathbf{y}}'$ axis by an angle α.

Section V displays typical patterns such as far-field beam patterns, and key radiation parameters for undistorted and various distorted IRIS configurations at L- and S-band. In Section VI, the results presented in this paper are summarized.

II. Surface Parameterization and PO Implementation

A. Parabolic Torus Surface Parameterization

To analyze a given reflector antenna geometry using PO [5], the surface parameterization ($z = f(x, y)$) and the normal vector of the surface must be known. The surface description of the PTRA is obtained by rotating a tilted parabola about the axis of rotation and expressing the surface representation in the reflector coordinate system [6] as shown in Fig. 3. In the following the derivation of the surface representation is outlined.

Fig. 3 displays a parabola tilted about the $\hat{\mathbf{y}}'$ axis by an angle α. The apex of the parabola is offset from the origin by $(d+f)$. In this paper, the variable d is referred to as the focus offset from the rotation axis, whereas f denotes the focal length of the parabola. The relationship between the membrane (primed) and the reflector (unprimed) coordinate system is given by

$$\begin{bmatrix} x \\ y \\ z \end{bmatrix} = \begin{bmatrix} \cos\alpha & 0 & -\sin\alpha \\ 0 & 1 & 0 \\ \sin\alpha & 0 & \cos\alpha \end{bmatrix} \cdot \begin{bmatrix} x' \\ y' \\ z' \end{bmatrix}. \tag{1}$$

A parabola in the unprimed coordinate system, offset by $(d+f)$ from the origin, is given by

$$z = (d+f) - \frac{x^2}{4f}. \tag{2}$$

In terms of the primed coordinate system this parabola is expressed using (1) as

$$(x' \sin\alpha + z' \cos\alpha) = (d+f) - \frac{1}{4f}(x' \cos\alpha - z' \sin\alpha)^2. \tag{3}$$

Rotation of the tilted parabola about the $\hat{\mathbf{z}}'$-axis ($x' \rightarrow \sqrt{(x')^2 + (y')^2}$) creates a body of revolution, i.e., the parabolic torus with torus tilt angle α. Using (1), one can again

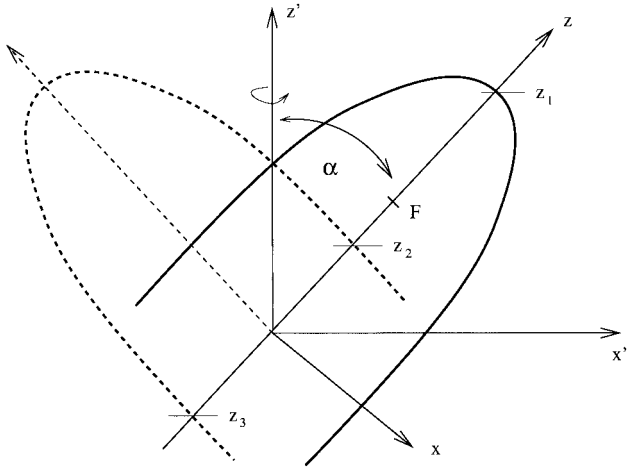

Fig. 4. Vertical cross section through a parabolic torus, depicting three solutions (z_1, z_2, and z_3) of the defining polynomial in (5).

express (3) in unprimed coordinates as

$$\left(\sqrt{(x\cos\alpha+z\sin\alpha)^2+y^2}\right)\sin\alpha + (-x\sin\alpha+z\cos\alpha)\cos\alpha = (d+f)-\frac{1}{4f}\left[\left(\sqrt{(x\cos\alpha+z\sin\alpha)^2+y^2}\right)\cos\alpha - (-x\sin\alpha+z\cos\alpha)\sin\alpha\right]^2. \quad (4)$$

Equation (4) is ordered, squared and reordered in terms of z, which yields a fourth order polynomial. The coefficient of the fourth-order term is identically zero; hence, the fourth-order polynomial reduces to a third order, which is given as

$$p_3z^3+p_2z^2+p_1z+p_0=0 \quad (5)$$

where the coefficients are detailed in the Appendix.

Fig. 4 depicts a vertical cross section through the axis of rotation, showing two intersecting parabolas for a candidate geometry. Only z_1 gives the correct solution for (5). The other two solutions z_2 and z_3 are created by the rotation about the $\hat{\mathbf{z}}'$-axis.

For the special case of $\alpha = 90°$, (5) reduces to a second-order polynomial, which is a more commonly used form of parabolic torus [7]. In this case, the surface representation and its partial derivatives are then defined explicitly as

$$z=\sqrt{(d+f)^2-(d+f)\frac{x^2}{2f}+\frac{x^4}{16f^2}-y^2} \quad (6a)$$

$$z_x=\frac{x^3/(8f^2)-(d+f)x/(2f)}{\sqrt{(d+f)^2-(d+f)\frac{x^2}{2f}+\frac{x^4}{16f^2}-y^2}} \quad (6b)$$

$$z_y=\frac{-y}{\sqrt{(d+f)^2-(d+f)\frac{x^2}{2f}+\frac{x^4}{16f^2}-y^2}}. \quad (6c)$$

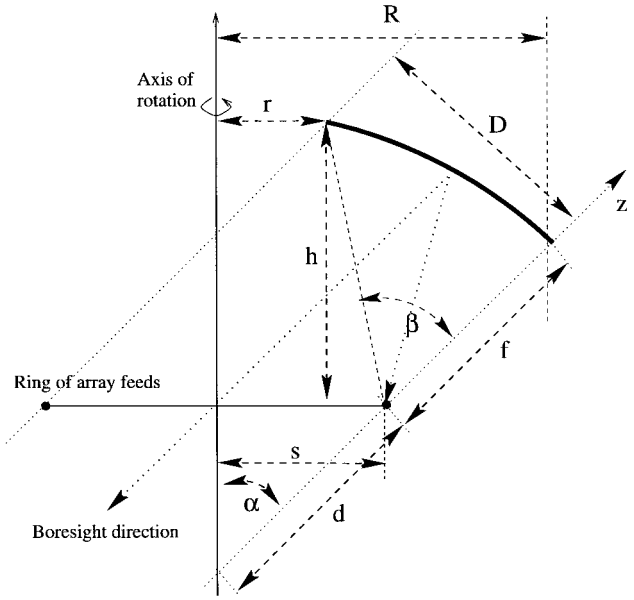

Fig. 5. Key geometrical parameters of IRIS.

For a tilt angle of $\alpha = 0°$, (5) reduces to the expected paraboloidal equation

$$z=(d+f)-\frac{x^2+y^2}{4f}. \quad (7)$$

B. PO Implementation

For a reflector antenna surface expressed by $(z = f(x, y))$, the induced PO current due to an incident field is given by

$$\mathbf{J}=2\hat{\mathbf{n}}\times\mathbf{H}_{\text{inc}} \quad (8)$$

where $\hat{\mathbf{n}}$ is the unit normal vector of the surface. Using the vector potential construction, the scattered fields due to this induced current can be readily determined [5]. In general, local reflection coefficient dyadics may be used to represent the reflection properties of the surface, which can be different from a perfectly conducting surface.

Applying the far-field approximation, the scattered far fields become

$$\mathbf{E}=-\frac{jk^2}{\omega\varepsilon}\frac{\exp(-jkr)}{4\pi r}(\bar{\bar{\mathbf{I}}}-\hat{\mathbf{r}}\hat{\mathbf{r}})\cdot\mathbf{T}(\theta,\varphi) \quad (9)$$

with

$$\mathbf{T}(\theta,\varphi)=\int_\Sigma \mathbf{J}(\mathbf{r}')\exp(jk\mathbf{r}'\cdot\hat{\mathbf{r}})\,ds' \quad (10)$$

where the PO current $\mathbf{J}(\mathbf{r}')$ has its support over the reflector surface. In order to find the PO current in (8), a surface description $[z = f(x, y)]$ and the surface normal $(\mathbf{n})$ with respect to the reflector coordinate system is needed. Equation (5) and its solution z_1 defines the surface. The partial derivatives of (5) are given by

$$z_x=-\frac{p_{3x}z^3+p_{2x}z^2+p_{1x}z+p_{0x}}{3p_3z^2+2p_2z+p_1}$$

$$z_y=-\frac{p_{3y}z^3+p_{2y}z^2+p_{1y}z+p_{0y}}{3p_3z^2+2p_2z+p_1}$$

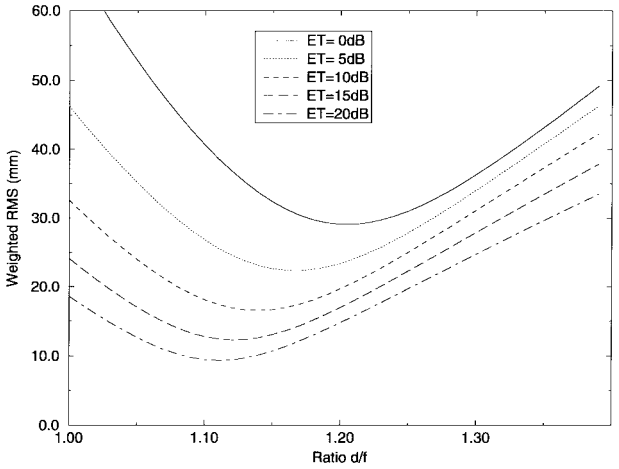

Fig. 6. Weighted rms, between a parabolic torus surface and a paraboloidal surface, versus relative focus offset ratio d/f. $\alpha = 35°$.

where $p_{ix} = \partial p_i/\partial x$ and $p_{iy} = \partial p_i/\partial y$ and the surface normal becomes

$$\mathbf{n} = [z_x, \quad z_y, \quad -1]^T \tag{11}$$

where T is the transpose operator. Note that this surface normal vector points toward the origin of the coordinate system in Fig. 3.

III. Torus Reflector Antenna Design

A. Reflector Antenna

For the design of IRIS, it became necessary to use a torus tilt angle $\alpha = 35°$ and a maximum outer diameter of the reflector membrane $2R = 25$ m (see Fig. 1). A sketch displaying the key geometrical parameters of IRIS is given in Fig. 5. Choosing $q = d/f$ as a design parameter, the aperture diameter D is obtained from the overall antenna diameter $2R$

$$D = 2R\frac{\cos\alpha}{1+1/q}. \tag{12}$$

The remaining key geometrical parameters, which allow proper mechanical representation of the antenna configuration, as shown in Fig. 5, can be determined using

$$s = \frac{D}{2\cos\alpha} \tag{13a}$$

$$d = \frac{s}{\sin\alpha} = \frac{D}{2\sin\alpha\cos\alpha} \tag{13b}$$

$$f = d/q \tag{13c}$$

$$\beta = 2\tan^{-1}\frac{D}{2f} \tag{13d}$$

$$r = s - \sin(\beta-\alpha)\frac{2f}{1+\cos\beta} \tag{13e}$$

$$h = \cos(\beta-\alpha)\frac{2f}{1+\cos\beta}. \tag{13f}$$

The reflector is offset fed to reduce the blockage effects due to the array feeds located at the focal ring. The focal ring is projected along the focal axis and the outline of its intersection with the reflector membrane defines the effective subradiating aperture. With the focal ring being circular, the projection onto the membrane surface yields an elliptical outline. The focus offset is found from (13b). The remaining parameters described in (13) are found in a similar and successive fashion.

To choose the optimum value of $q = d/f$ for the most desired far-field pattern characteristics, parametric studies have been conducted. This was done using both the root mean square (rms) of the surface deviation of IRIS to a best fit paraboloid and the evaluation of the radiation characteristics of IRIS from (9). Fig. 6 displays the weighted rms of the surface deviation versus d/f ratio. The weighting of the surface deviation is done to simulate the effect of the nonuniform illumination of the reflector aperture by the array feed, i.e., the edge taper. For larger edge tapers, the minimum of the rms curves is shifted toward smaller d/f. The optimum ratio for an edge taper of -15 dB is at $d/f = 1.11$. The same result was obtained independently by maximizing the calculated boresight directivity as a function of d/f ratio. Similar to spherical reflectors, the ratio between focal length and sphere radius influences the surface deviation from a best fit paraboloid and, hence, its radiation performance [8]. The rms is defined here as the square root of the sum of the square of the demeaned surface deviation.

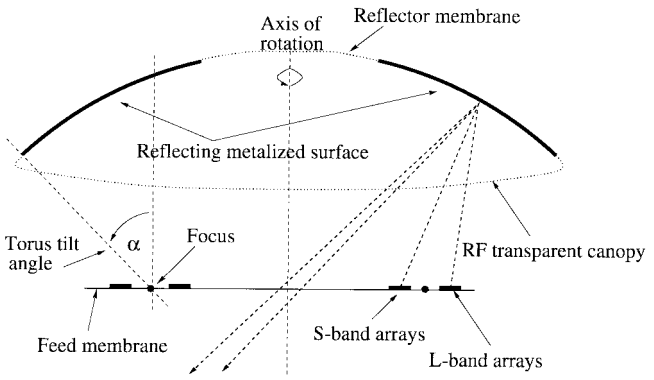

Fig. 7. L-band and S-band array placements along the feed membrane.

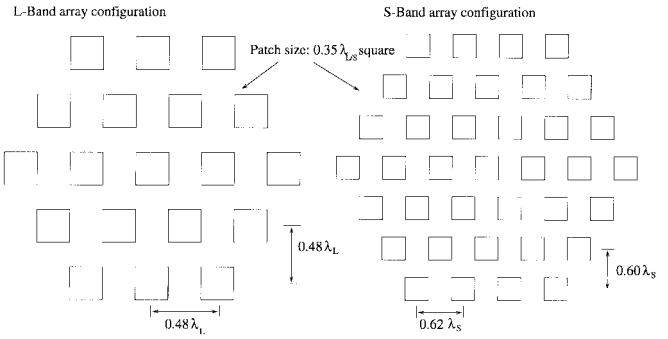

Fig. 8. Geometry of the triangular microstrip patch antenna arrays at L-band and S-band. $\lambda_L = 214$ mm, and $\lambda_S = 117$ mm.

B. Array Feeds

To allow for dual frequency operation of IRIS, microstrip array feeds at L-band (19 elements) and at S-band (37 elements) have been proposed. As seen in Fig. 7, the array feeds are placed on the feed membrane and offset from the focal

TABLE I
GEOMETRICAL PARAMETERS OF THE IRIS CONFIGURATION

Outer reflector membrane radius	R	$= 12.5$ m
Tilt angle	α	$= 35°$
Reflector diameter (Elevation)	D	$= 10.77$ m
Focal length	f	$= 10.33$ m
Focus offset	d	$= 11.46$ m
Focal ring radius	s	$= 6.58$ m
Membrane height	h	$= 12.34$ m
Inner radius	r	$= 2.06$ m
Feed displacement (L-band)	δ_L	$= 0.26$ m
Array beam tilt (L-band)	θ_L	$= 4.21°$
Array phasing (L-band)	$\Delta\varphi_L$	$= 12.7°$
Feed displacement (S-band)	δ_S	$= 0.24$ m
Array beam tilt (S-band)	θ_S	$= 7.19°$
Array phasing (S-band)	$\Delta\varphi_S$	$= 27.0°$

ring. Both array feeds are triangular based. With respect to the axis of rotation the S-band array feed is placed inside and the L-band array feed is placed outside of the focal ring. Both array feeds are progressively phased ($\Delta\varphi$) between rows to tilt their beams toward the center of the reflector.

Fig. 8 displays a sketch of the geometry of the triangular microstrip patch antenna arrays at L-band and S-band. The element patch size is $0.35\lambda_{L/S} \times 0.35\lambda_{L/S}$, where λ_L and λ_S is the wavelength at L-band and S-band, respectively. The excitation coefficients for the L-band array are chosen in a way to provide an approximate edge taper of -15 dB. At S-band the array severely under illuminates the reflector surface in order to create a similar beamwidth as the L-band beamwidth of approximately 1.3°.

With the selected values for R and α and the application of (12) and (13), the geometrical parameters of IRIS are completely determined as summarized in Table I.

IV. DISTORTION MODELS OF INFLATABLE PARABOLIC TORUS REFLECTORS

The systematic surface distortions affecting IRIS performance are determined by the inflatable membrane and its supporting structure. Detailed analysis of the inflatable reflector membrane using both finite-element models and the results of recent measurements of some of the existing inflatable structures have revealed that these distortions have W- or M-shaped profiles [2]. For torus surfaces, the surface distortions have a strong functional dependency in elevation, while being almost rotationally symmetric (azimuthal direction) about the $\hat{\mathbf{z}}'$ axis. In the following this class of distortions is abbreviated as *elevation distortion.* The functional dependency in the elevation has been assumed to be of the form

$$\Delta r = \varepsilon \cos\left(2\pi N \frac{\theta'}{\alpha}\right) \tag{14}$$

where N denotes the periodicity of the distortion in the range $0 \leq \theta' \leq \alpha$, ε the center-to-peak height, and α the torus tilt angle. Δr marks the displacement in $\hat{\mathbf{r}}'$ direction, where

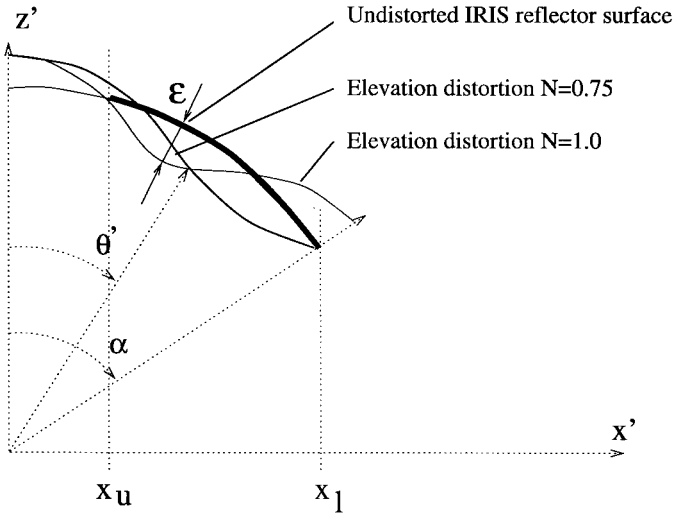

Fig. 9. Vertical cross section through the axis of rotation of IRIS, displaying a candidate elevation surface distortion with periodicities of $N = 0.75$ and $N = 1.0$.

TABLE II
RF CHARACTERISTICS OF IRIS

Configuration	D (dB)	XP (dB)	BT (°)	BW (°)	BE (%)
L, undistorted	42.4	15.9	1.1	1.39	90
S, undistorted	44.4	13.7	-1.3	1.21	97
L, $N = 0.75$, $\varepsilon = 10$ mm	42.1	15.7	1.0	1.41	89
S, $N = 0.75$, $\varepsilon = 10$ mm	44.3	13.6	-1.4	1.16	97
L, $N = 1.0$, $\varepsilon = 10$ mm	42.1	15.9	1.3	1.41	88
S, $N = 1.0$, $\varepsilon = 10$ mm	44.2	14.1	-1.0	1.15	97
L, hotmax	42.2	15.9	1.0	1.36	89
S, hotmax	44.5	13.8	-1.4	1.07	97
L, coldmin	42.4	15.9	1.1	1.34	89
S, coldmin	44.5	13.8	-1.3	1.01	96

$\hat{\mathbf{r}}'$ is the unit vector in the radial direction in the membrane (primed) coordinate system.

Fig. 9 displays a cross section through the axis of rotation of IRIS. The undistorted reflector surface is shown along with candidate distortion with a functional dependency in elevation. For these distortions periodicities of $N = 0.75$ and $N = 1.0$ have been chosen.

The distortion displayed in Fig. 9 is slowly varying in nature. With tapered illumination, the surface distortion in the center of the aperture dominantly affects the reflector radiation characteristics. Depending on the absolute height and the periodicity of the surface distortion, the beam may be tilted in elevation. The direction and the amount of this undesirable beam tilt is dependent on both the periodicity and the height of the surface distortion.

Structural distortions of the feed membrane and misplacement and misalignment of the feed membrane, with respect to the reflector membrane, cause an effective feed defocusing and have to be considered in addition to the reflector membrane surface distortion. For IRIS, both the amount of axial and lateral feed displacement was considered. Given a stringent beam pointing error budget of 0.125° for IRIS, the lateral

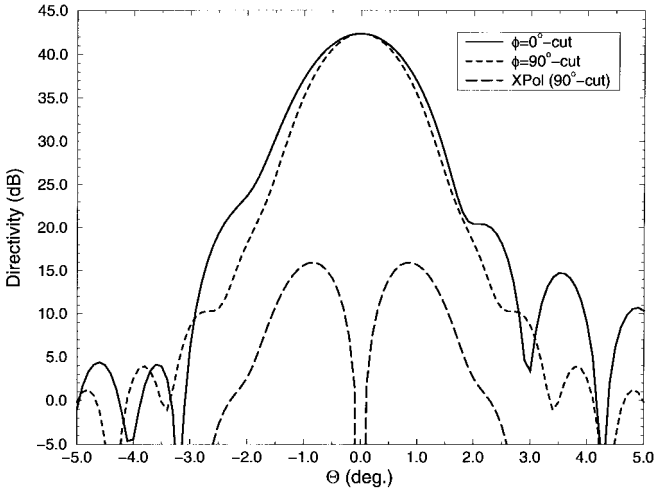

(a)

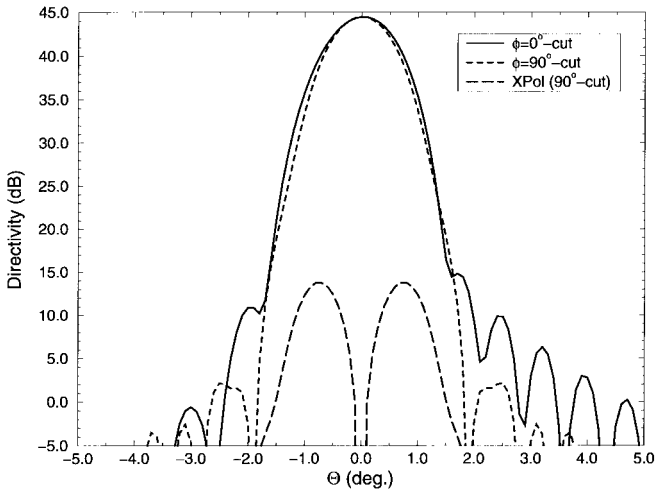

(b)

Fig. 10. Far-field pattern for $\varphi = 0°$ and $\varphi = 90°$ cuts, cross polarization in the $\varphi = 90°$ cut. No surface distortions. (a) L-band and (b) S-band.

displacement tolerances of the array feeds with respect to the reflector membrane are in the order of $\Delta = 22.5$ mm. Additionally, random surface errors have to be considered as a further source of deterioration of the radiation performance. Their effects on the boresight directivity can be estimated by Ruze's equation [9], [10].

V. Radiation Performance

In the following the far-field pattern of IRIS at both L-band and S-band are presented. The figures show the far-field pattern in the two principal cuts and the cross polarization in the $\varphi = 90°$ cut. Their key radiation parameters are listed in Table II. The parameters shown are the directivity D, the cross polarization XP, beam tilt BT, beamwidth BW, and beam efficiency BE.

The beam efficiency is defined as

$$BE = \frac{\text{radiated power in solid angle } 2\theta_0}{\text{total radiated power}}$$

where the null-to-null beamwidth for the beam efficiency computation is typically determined from the 3-dB beamwidth

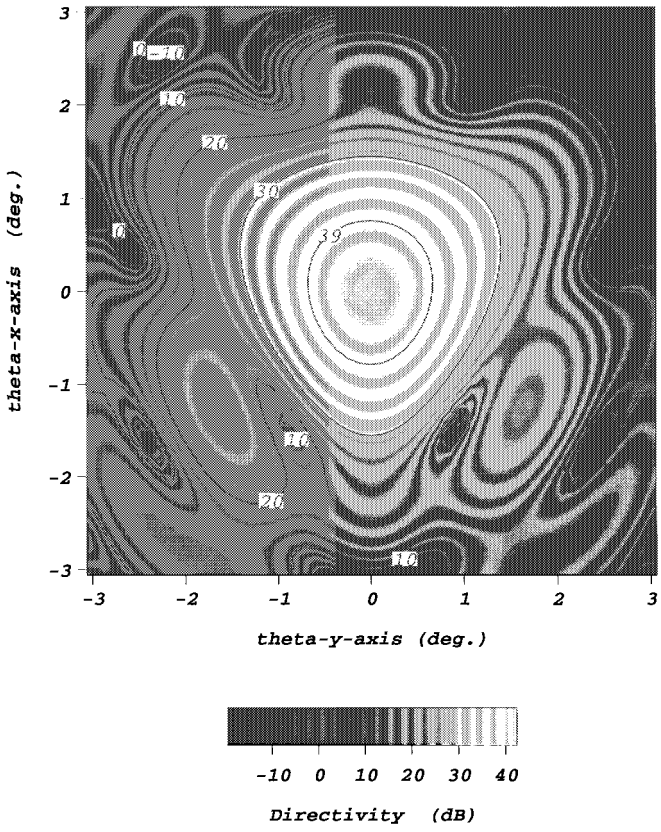

(a)

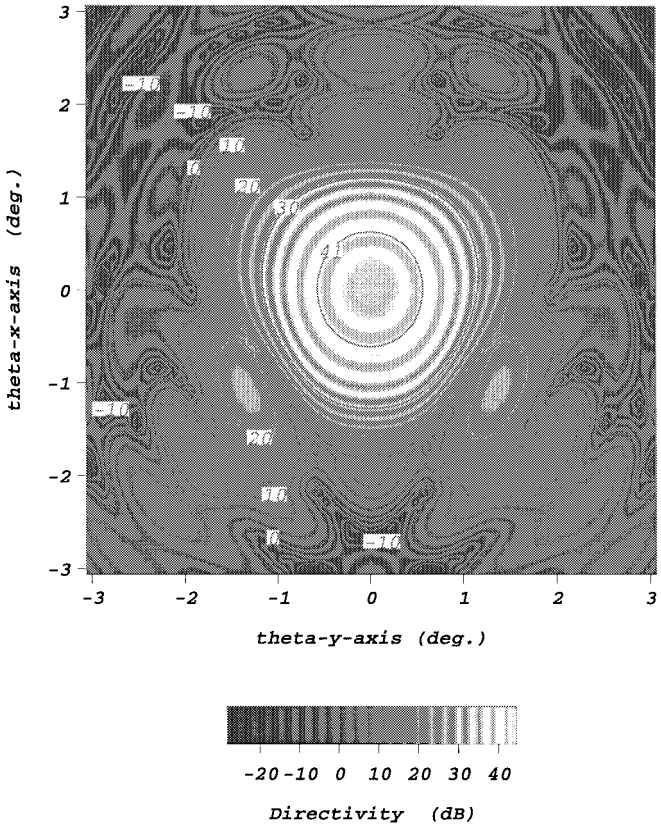

(b)

Fig. 11. Beam contour pattern with $\theta_x = \theta \cos \varphi$, $\theta_y = \theta \sin \varphi$. No surface distortions. (a) L-band and (b) S-band.

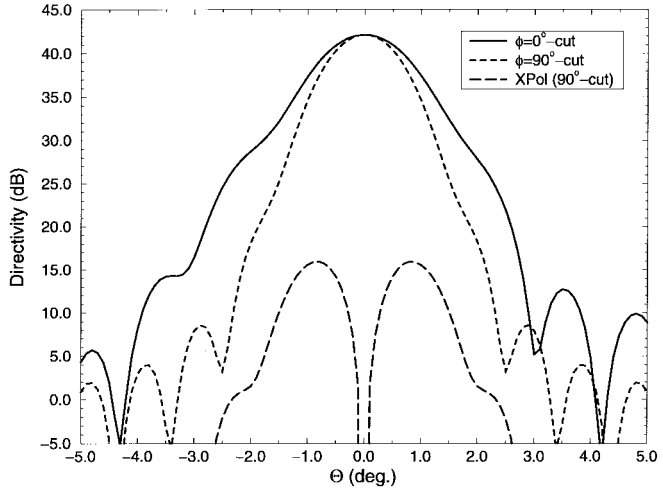

(a)

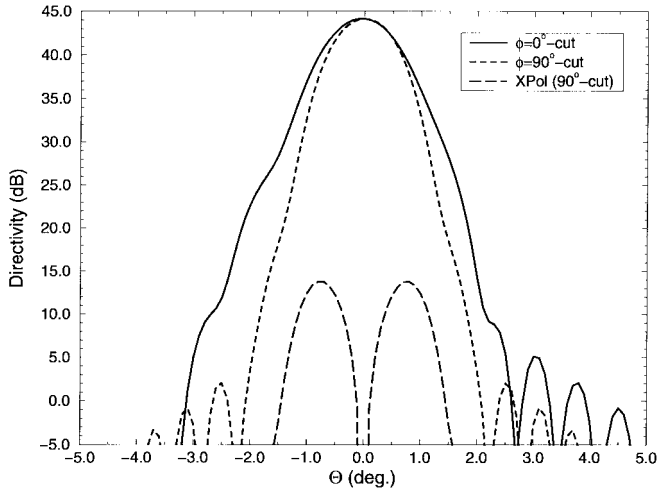

(b)

Fig. 12. Far-field pattern for $\varphi = 0^\circ$ and $\varphi = 90^\circ$ cuts, cross polarization in the $\varphi = 90^\circ$ cut. Surface distortion with $N = 1$ and $\varepsilon = 10$ mm. (a) L-band. (b) S-band.

[11], [12], using

$$BW_{\text{Null-to-Null}} = 2.5 \times BW_{3\,\text{dB}}.$$

θ_0 is the angle measured from boresight to approximately the first null, where $BW_{3\,\text{dB}}$ was taken to be the average of the beamwidths obtained from the principal cuts and $\theta_0 = BW_{\text{Null-to-Null}}/2$.

Fig. 10(a) and (b) display the far-field pattern of the undistorted IRIS at (a) L-band and (b) S-band, respectively. The beam tilt is caused by the displacement of the array feeds to allow for the dual frequency operation. Fig. 11(a) and (b) display the beam contour pattern of IRIS at L-band and S-band, respectively. It is interesting to observe the typical triangular shaped main beam characteristic of the torus reflector antenna.

Fig. 12(a) and (b) display the far-field pattern of IRIS deteriorated by an elevation distortion with $N = 1.0$ and $\varepsilon = 10$ mm. The higher periodicity of the distortion causes the beam tilt to become larger and the performance to degrade more severely. Note that the direction of the beam tilt changes

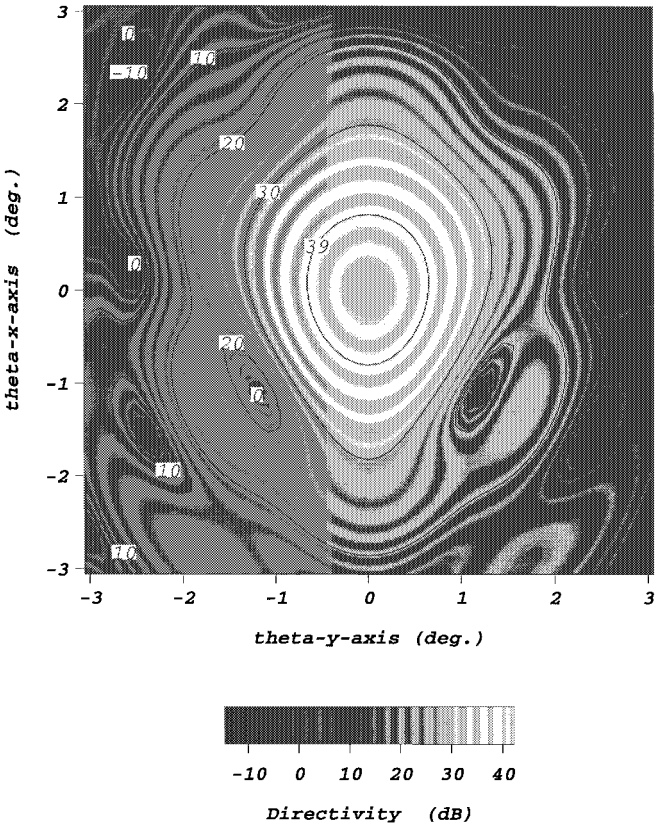

(a)

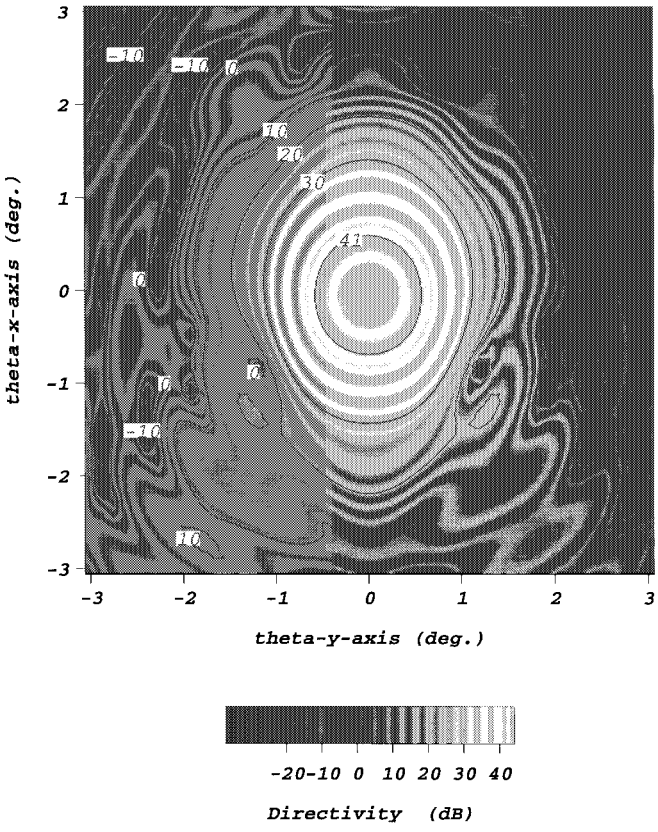

(b)

Fig. 13. Beam contour pattern with $\theta_x = \theta \cos \varphi$, $\theta_y = \theta \sin \varphi$. Surface distortion with $N = 1$ and $\varepsilon = 10$ mm. (a) L-band. (b) S-band.

with the change of periodicity. Fig. 13(a) and (b) display the beam contour pattern for IRIS with an elevation distortion ($N = 1.0$, $\varepsilon = 10$ mm) at L-band and S-band, respectively. Compared to Fig. 11 the triangular beam shapes are not as confined for the distorted geometry, also the level of energy surrounding the main beam regions is increased.

During one orbital encirclement of the earth, IRIS is subject to some thermal changes. The temperature gradient across the structure causes a deformation, which has similar effects on the radiation characteristics as the simulated elevation distortion. At the two extreme temperature points (*coldmin* for the lowest and *hotmax* for the highest temperature), the overall surface deformation of the reflector membrane has been simulated and tabulated. For the PO analysis program, these nonuniformly spaced surface data points were interpolated using a polynomial least square interpolation technique to obtain both the surface description $(f(x, y))$ and the surface normal vector $(\mathbf{n})$ [3].

Fig. 14(a) and (b) display the beam contour pattern for the thermal distortion denoted by *hotmax* for L-band and S-band, respectively. The thermal distortion at both extreme temperatures shows radiation characteristics similar to the distorted radiation pattern displayed in Fig. 13. It is worthwhile to mention that the sidelobe structure is more affected by this class of surface distortion than by the mechanical distortions displayed in Fig. 13.

Table II displays the key radiation parameters of the IRIS configuration. The requirements for the IRIS radiation characteristics have been met. Both beam efficiency and cross polarization remain well above their required margin of 85% and a cross-polarization isolation of 18 dB, respectively.

Similarly, Table II shows that the assumed worst-case distortion ($\varepsilon = 10$ mm for $N = 1.0$) as well as the simulated thermal distortion affect the radiation performance. While the beam efficiency remains safely above the required limit for these distortions, the beam tilts by 0.1°, which is about 8% of the beamwidth. For a beam pointing error budget of less than 0.125°, the induced beam tilt dominates the deteriorating effects on the radiation performance; hence, the requirements on fabrication accuracy and errors induced by the deployment process.

Distortion compensation using corrective feed array excitation coefficients provides a possibility [13] to correct for the undesirable beam tilt and research into methods to determine these coefficients is currently in progress.

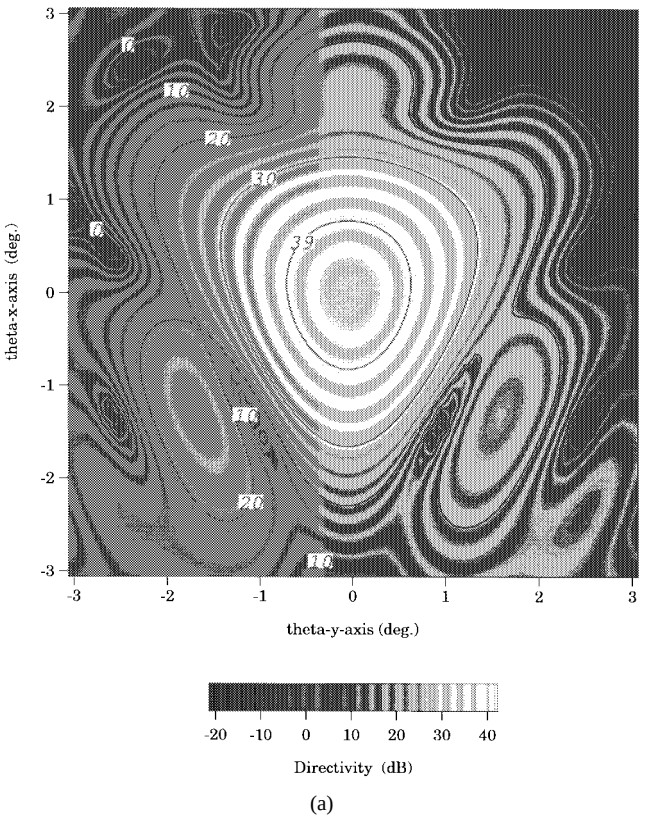

(a)

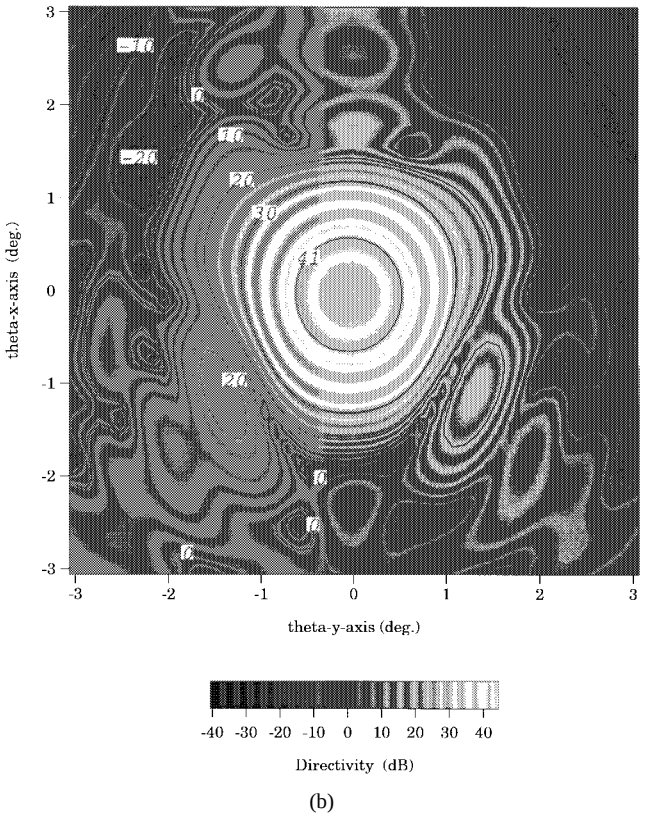

(b)

Fig. 14. Beam contour pattern with $\theta_x = \theta \cos \varphi$, $\theta_y = \theta \sin \varphi$. Hotmax surface distortion case. (a) L-band. (b) S-band.

VI. Conclusions

In this paper, the electromagnetic characteristics of an inflatable offset parabolic torus reflector antenna based on the geometrical specifications of the soil moisture radiation mission have been analyzed. The design of a multibeam parabolic torus reflector antenna using inflatable antenna technology has been outlined. Parametric studies have been presented to find the most suitable design parameters. A general distortion model suitable for the antenna material properties (inflatable antenna) and antenna geometry (parabolic torus) has been developed to predict the antenna radiation characteristics under operational environment. Representative RF parameters have been provided for undistorted and distorted reflector geometry. Finally, the capability to accurately analyze and

model complex inflatable reflector antenna structures has been demonstrated.

APPENDIX
COEFFICIENTS OF THE POLYNOMIAL DEFINING THE PTRA SURFACE

The coefficients of the polynomial in (5) are defined by

$$\begin{aligned} p_0 &= (b_0 r_0 - t_0^2) \\ p_1 &= (b_0 r_1 + b_1 r_0 - 2t_0 t_1) \\ p_2 &= (b_1 r_1 + b_0 r_2 + b_2 r_0 - t_1^2 - 2t_0 t_2) \\ p_3 &= b_1 r_2 + b_2 r_1 - 2t_1 t_2 \end{aligned}$$

where

$$\begin{aligned} r_0 &= 4 \sin^2 \alpha \left(2f + \frac{x}{2} \sin(2\alpha)\right)^2 \\ r_1 &= -2 \sin^2(2\alpha) \left(2f + \frac{x}{2} \sin(2\alpha)\right) \\ r_2 &= \sin^2(2\alpha) \cos^2 \alpha \\ b_0 &= x^2 \cos^2 \alpha + y^2 \\ b_1 &= x \sin 2\alpha \\ b_2 &= \sin^2 \alpha \\ t_0 &= 4f(d+f) + 2fx \sin(2\alpha) \\ &\quad - x^2(\cos^4 \alpha + \sin^4 \alpha) - y^2 \cos^2 \alpha \\ t_1 &= -4f \cos^2 \alpha - \frac{x}{2} \sin(4\alpha) \\ t_2 &= -\frac{1}{2} \sin^2(2\alpha). \end{aligned}$$

The geometrical parameters α, f, and d used in the above equations are defined in Fig. 5.

ACKNOWLEDGMENT

The authors would like to thank E. Njoku, W. Williams, J. Sercel, and R. Freeland of JPL, Pasadena, CA, for their support of this project at UCLA and their very constructive discussions throughout the completion of this project. Additionally, useful input from L'Garde engineers on the topic of the inflatable reflector antenna technology is appreciated.

REFERENCES

[1] E. Njoku, Y. Rahmat-Samii, W. Wilson, and J. Sercel, *Radiometer Workshop.* Boston, MA: Nov. 1996.

[2] R. Freeland, S. Bard, G. Veal, G. Bilyeu, C. Cassapakis, T. Campbell, and M. C. Bailey, "Inflatable antenna technology with preliminary shuttle experiment results and potential applications," in *AMTA96*, Seattle, WA, Oct. 1996, pp. 3–8.

[3] Y. Rahmat-Samii, "Effects of deterministic surface distortions on reflector antenna performace," *Antennes Télécommunication*, vol. 40, no. 7/8, pp. 350–360, 1985.

[4] A. Roderer and Y. Rahmat-Samii, "Unfurlable satellite antennas: A review," *Annal. Telecommunicat.*, vol. 44, no. 9/10, pp. 475–488, Nov. 1989.

[5] Y. Rahmat-Samii, "Reflector antennas," in *Antenna Handbook*, Y. T. Lo and S. W. Lee, Eds. New York: Van Nostrand Reinhold, 1988, ch 15.

[6] A. G. P. Boswell, "The parabolic torus reflector antenna," *The Marconi Review*, fourth quarter, pp. 237–248, 1978.

[7] K. S. Kelleher, "A new wide-angle microwave reflector," Tele-Tech Eletron. Indust., June 1953.

[8] Y. Rahmat-Samii and V. Galindo-Israel, "Shaped reflector antenna analysis using the Jakobi–Bessel series," *IEEE Trans. Antennas Propagat.*, vol. AP-28, pp. 425–435, July 1980.

[9] J. Ruze, "Antenna tolerance theory," *Proc. IEEE*, vol. 54, pp. 633–640, Apr. 1966.

[10] Y. Rahmat-Samii, "An efficient computational method for characterizing the effects of random surface errors on the average power pattern of reflectors," *IEEE Trans. Antennas Propagat.*, vol. 31, pp 92–98, Jan. 1983.

[11] M. L. Zimmermann, "Computation and optimization of beam efficiency for reflector antennas," *Electromagn.*, vol. 11, pp. 235–254, 1991.

[12] B. Shen and W. L. Stutzmann, "Performance evaluation of high-gain radiometer antennas," *Radio Sci.*, vol. 30, no. 6, pp. 1767–1776, Nov.–Dec. 1995.

[13] Y. Rahmat-Samii, "Array feeds for reflector surface distortion: Concepts and implementation," *IEEE Antennas Propagat. Mag.*, vol. 32, pp. 20–26, Aug. 1990.

Robert A. Hoferer (S'96) was born in Offenburg, Germany, on December 13, 1968. He received the Dipl.Ing. (M.S.E.E.) degree from the University of Karlsruhe, Germany, in 1994. He is currently working toward the Ph.D. degree at the ARAM Laboratory, University of California, Los Angeles.

In 1994, he spent a six-month internship at the Antenna Research, Analysis, and Measurement Laboratory (ARAM) at the University of California, Los Angeles (UCLA) to conduct research for his diploma thesis on focal plane sampling of reflector antennas for surface distortion analysis. He is working as a Graduate Research Associate at the ARAM Laboratory, UCLA. His research interests include numerical electromagnetics, antenna design, diffraction analysis, and synthesis of reflector antennas.

Mr. Hoferer was awarded the third prize in the student paper competition at the URSI National Radio Science Meeting in 1998.

Yahya Rahmat-Samii (S'73–M'75–SM'79–F'85), for a photograph and biography, see p. 748 of the June 1998 issue of this TRANSACTIONS.